PERGAMON

Renewable and Sustainable Energy Reviews
2 (1998) 287–301

RENEWABLE
& SUSTAINABLE
ENERGY REVIEWS

# Flow and heat transfer in the air gap behind photovoltaic panels

B. Moshfegh[a,*], M.Sandberg[b]

[a] *Division of Energy and Production Systems, Department of Technology, University College of Gävle/Sandviken, S-801 76 Gävle, Sweden*
[b] *Department of Built Environment, Royal Institute of Technology, KTH, S-801 02 Gävle, Sweden*

Received 3 March 1998; accepted 28 April 1998

**Abstract**

The impetus of this paper is to analyse numerically and experimentally the flow and heat transfer characteristics of buoyancy-driven air convection behind photovoltaic panels. Both convection and radiation heat exchanges are considered as the heat transfer mechanisms by which the thermal energy is transferred into the air. Numerical and experimental results are obtained for a channel of 7.0 m in height and the channel walls are separated by a distance of 0.23 m. In the experiment heat is supplied to the air gap from heating foil attached to one of the vertical walls. Different input heat fluxes and emissivity of the bounding surfaces are considered in order to show their effect on the heat transfer across the air layer. Detailed studies of the flow and thermal fields in the air are presented in order to explore the thermal behaviour of the air in the channel. Velocity and temperature profiles of the outlet air and the surface temperature of the heated and insulated wall is presented. The numerical results agreed well with the experimental measurements. 

*Key words:* Photovoltaic panels; Turbulent flow; Heat transfer; Vertical channel; Natural convection; Radiation

## Nomenclature

$A$ area
$B$ specific buoyancy flux
$C_p$ specific heat
$d$ wall-to-wall distance
$F$ shape factor
$g$ acceleration due to gravity

* Corresponding author. Tel.: 0046 26 64 8804; fax: 0046 26 64 8828; e-mail: bmh@hgs.se

1364–0321/98/$ - see front matter 
PII: S1364–0321(98)00005–7

$G_k$ buoyant production of $k$
$h$ convective heat transfer
$H$ height
$k$ turbulent kinetic energy
$k$ friction factor, see eqn (13)
$n$ surface unit normal vector
$q$ total amount of heat
$q''$ heat flux
$q''_{in}$ uniform input heat flux
$p$ pressure
$P_k$ shear production of $k$
$Pr$ Prandtl number
$Ra$ Rayleigh number
$T$ temperature
$w$ width of the air gap
$u, v$ velocity components in the $x$-, $y$-direction
$U$ flow average velocity
$x, y$ co-ordinates in the Cartesian system

*Greek symbols*
$\alpha$ configuration factor
$\alpha_H$ thermal diffusivity
$\beta$ thermal expansion coefficient
$\delta$ Kronecker delta
$\varepsilon$ emissivity
$\varepsilon$ turbulent energy dissipation rate, see eqn (8)
$\lambda$ thermal conductivity
$\lambda$ friction factor
$\mu$ dynamic viscosity
$\nu$ kinematic viscosity
$\rho$ density
$\sigma$ Stefan-Boltzmann constant

*Subscripts*
a ambient
c insulated wall
conv convection
entr entrance
h heated wall
i inlet
o outlet
rad radiation
t turbulent

## 1. Introduction

The solar cell operation is based on the ability of semiconductors to convert sunlight into electricity by exploiting the *photovoltaic effect*. There is a growing interest in

studying heat and mass flow in air gaps behind Photovoltaic panels (PV). One impetus for this type of work is the interest in hybrid systems (i.e. the combined generation of heat and electricity). A hybrid system consists of a PV panel with a cavity (air gap) between the PV panel and the building fabric. This air gap is a natural draft 'chimney' and the flow in the air gap is driven by buoyancy (heat) and the wind-induced pressure difference between the top and bottom of this chimney. The PV panel is heated by the incident solar radiation and from the PV panel heat is transferred to the air gap by convection and radiation. Radiative heat transfer carries energy across the air gap. The net radiation, absorbed by the otherwise unheated wall, is in turn, transferred to the fluid by convection. Thus radiation activates convection on the otherwise unheated surface.

Another impetus is the fact that by reducing the solar cell temperature the efficiency of the cells will increase. The efficiency of some types of solar cells is very much dependent on the operating temperature of the cell. For example *the relative temperature coefficient* of crystalline silicon solar modules is in the range 0.4–0.6% K. With 13% absolute conversion efficiency this corresponds to an absolute temperature coefficient between 0.031 and 0.046% K. Therefore a reduction by 20°C will give an increase in efficiency between 0.6 and 1%.

As a result, knowledge enlightening the actual physical conditions in air gaps in ventilated facades is crucial for design engineers. The measurement conditions are very difficult due to the presence of strong temperature gradients and the exchange of heat between surfaces by radiation. At the same time the strong heat transfer mechanisms pose problems when using Computational Fluid Dynamics, CFD. In real buildings there are almost transient conditions and both the heat input to the air and the flow rate in the air gap vary with time. The instantaneous heat input to the air can hardly be measured. The approach taken in this study is to combine different techniques, CFD and experiments which shall be seen as complementary techniques. The basic approach is to seek solutions for simplified boundary conditions. For example, only stationary conditions are explored and the heat input to the air is controlled and known. In the CFD predictions the heat input is given as a boundary condition, while in the experiments the heat input is known by using a heating foil and a well insulated structure. The solutions for simple boundary conditions are asymptotic solutions to the more general transient cases occurring in real buildings and they will shed light on the range of conditions occurring in ventilated facades.

The techniques are complementary in the sense that for example detailed temperature profiles can be predicted by CFD but are difficult to measure. On the other hand, experiments can cope with transitional flows which CFD cannot.

## 2. Description of physical model

In studies of air flow and heat transfer between solar cells and the air gap in hybrid systems one can to some extent mimic the properties of solar panels by inserting a heating foil in an insulated channel. By choosing a thick insulation one can ensure that most of the heat generated by the heating foil is transferred to the air in the

channel. This approach enables a systematic study of the relation between input heat and various flow and heat transfer properties. A vertical channel with an air gap with dimensions, $w = 1.54$ m, $d = 0.23$ m, and height, $H = 6.5$ m is built in the Laboratory for Ventilation and Air Quality, at the Royal Institute of Technology, Gävle, Sweden. The channel is insulated with 0.29 m mineral wool. To minimise end effects the width of the heating foil is larger than the width of the air gap. The heating foil is 460 mm wide and 0.5 mm thick. The heating elements in the foil consist of electrically conducting transverse stripes 8 mm wide spaced 2 mm apart. The heating foils are attached with double adhesive tape. The heating foil covers the whole space of the walls. The heating foil is powered by a variable transformer. The electrical power supplied to each section is measured by means of a power transmitter which converts the electrical power to a voltage simply presented on a voltmeter. The relative error in recorded power, $P_{in}$, is assessed to be less than 2%. The tests are carried out for the heat fluxes, 20, 50, 100, 200 and 300 W/m$^2$, respectively.

The surface temperature on the walls is measured by means of foil thermocouples attached with double adhesive tape. Measuring of the air temperature between the walls is done by using small thermocouples made of 0.2 mm diameter wires. The error is 0.3°C absolute, and the relative error between measuring points is estimates to be less than 0.1°C.

The flow rate in the channel is measured by using tracer gas with the so called constant flow technique. Gas is introduced at the bottom of the channel with a known volume flow rate and the volume concentration at the exit is recorded. The concentration is read with an infrared gas analyser giving the volume concentration in parts per million [ppm]. Tracer gas technique is robust and accurate technique. A review of tracer gas techniques with a statement of the accuracy is given in Etheridge and Sandberg [1].

## 3. Description of numerical model

The geometry of the air gap and the relevant parameters, as well as the boundary conditions considered here are shown in Fig. 1. The origin of the rectangular Cartesian co-ordinate system $(x, y)$ is located on the bottom line of the channel entrance.

Vertical surfaces represent a heated wall with a height of 6.5 m exposed to a constant uniform input heat, $q''_{in}$, and an insulated 7.0 m high wall. The width of the walls is assumed to be large in comparison to other dimensions, thus the problem can be considered two-dimensional. The bottom surface is also well insulated and assumed to be a blackbody. The air enters at a temperature equal to the ambient temperature, $T_a$, at the lower left hand side and the buoyancy-induced flow passes over the heated and insulated walls and exits at the top of the gap. These are the realistic thermal boundary conditions which can be considered for the case presented in this study.

The flow is assumed to be steady with negligible viscous dissipation. The thermophysical properties of the air are assumed to be constant, except for the buoyancy term of the momentum equations, i.e. the Boussinesq approximation, see Gray et al.[2] The radiation surfaces are assumed to be grey-diffuse and the air does not

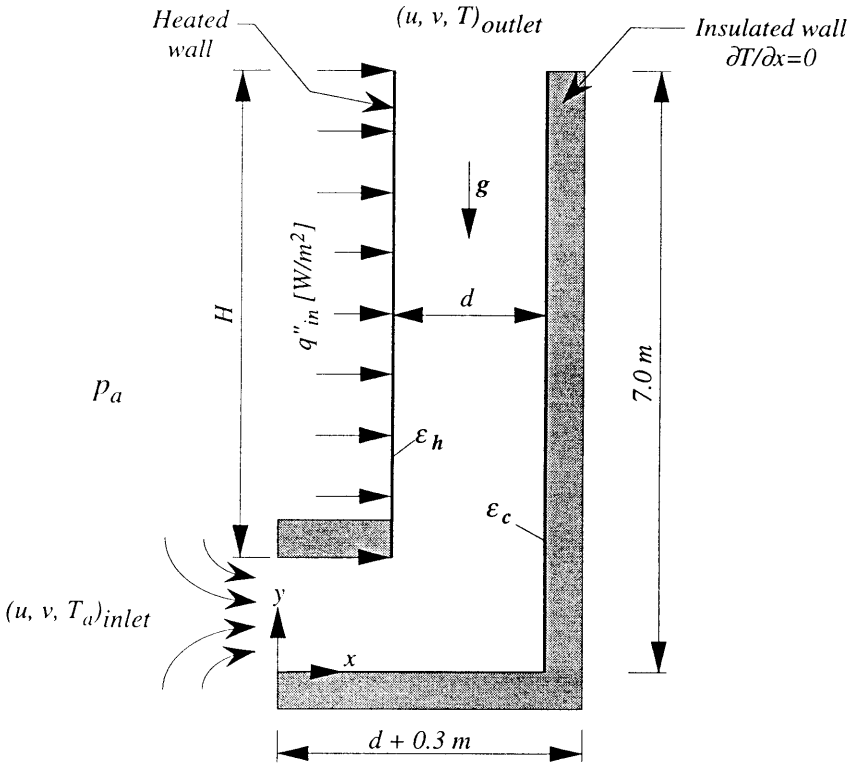


Fig. 1. Geometry and boundary conditions for the numerical model.

interact directly with the radiative process. On such modelling assumptions, the governing equations for conservation of mass, momentum, energy and turbulent kinetic energy as well as turbulent energy dissipation are obtained as follows:

Equation of the conservation of mass

$$\vec{\nabla}\cdot\vec{u} = 0 \tag{1}$$

Equation of the conservation of momentum

$$\rho\vec{\nabla}\cdot\vec{u}u = -\partial p/\partial x + \vec{\nabla}\cdot(\mu+\mu_t)\vec{\nabla}u + \vec{\nabla}\cdot(\mu+\mu_t)(\partial\vec{u}/\partial x) \tag{2}$$

$$\rho\vec{\nabla}\cdot\vec{u}v = -\partial p/\partial y - g\rho\beta(T-T_a) + \vec{\nabla}\cdot(\mu+\mu_t)\vec{\nabla}v + \vec{\nabla}\cdot(\mu+\mu_t)(\partial\vec{u}/\partial y) \tag{3}$$

Equation of the conservation of energy

$$\rho C_p\vec{\nabla}\cdot\vec{u}T = \vec{\nabla}\cdot(\lambda+\lambda_t)\vec{\nabla}T \tag{4}$$

where the heat transfer condition on each segment of the boundary of the fluid and the heat exchanged between radiating boundaries regardless of the fluid is calculated by:

$$q'' = -(\lambda \nabla T)n(s) = q''_{a}(s) + q''_{conv}(s) + q_{rad}(s) \tag{5}$$

$$\sum_{j=1}^{N} (\delta_{ij}/\varepsilon_j - F_{ij}(1-\varepsilon_j)/\varepsilon_j) q^j_{r} = \sum_{j=1}^{N} (\delta_{ij} - F_{ij}) \sigma T_j^4 \tag{6}$$

Equation of the transport of turbulent kinetic energy

$$\rho \vec{\nabla} \cdot \vec{u} k = \vec{\nabla} \cdot (\mu + \mu_t/\sigma_k) \vec{\nabla} k + P_k + G_k - \rho \varepsilon \tag{7}$$

Equation of the turbulent energy dissipation

$$\rho \vec{\nabla} \cdot \vec{u} \varepsilon = \vec{\nabla} \cdot (\mu + \mu_t/\sigma_\varepsilon) \vec{\nabla} \varepsilon + \left( C_1 \cdot P_k + C_1 (1 - C_3) G_k - C_2 \cdot \rho \varepsilon - \frac{C_\mu \eta^3 (1 - \eta/\eta_0) \varepsilon}{1 + \beta \eta^3} \right) \varepsilon / k \tag{8}$$

in which

$$\mu_t = \rho C_\mu k^2/\varepsilon, \quad \sigma_t = \mu_t C_p/\lambda_t, \quad P_k = \mu_t (2 \nabla \vec{u} \cdot \nabla \vec{u} + (\partial u/\partial y + \partial v/\partial x)^2)$$

$$G_k = \vec{g} \mu_t \beta \vec{\nabla} T/\sigma_t, \quad \eta = (P_k/\mu_t)^{0.5} k/\varepsilon$$

where the pressure defect $p$ is the difference between the channel and the ambient pressure at the same elevation, and $T_a$, is the ambient temperature taken as the reference temperature for this study. The following standard constants are used in the $k$-$\varepsilon$ model using the Renormalization Group, RNG method, see Yakot et al.[3]

$$C_\mu = 0.0865, \quad C_1 = 1.45, \quad C_2 = 1.83, \quad C_3 = 0.8, \quad \sigma_t = 0.9,$$

$$\sigma_k = 0.8, \quad \sigma_\varepsilon = 1.15, \quad \kappa = 0.41, \quad \beta = 0.1695, \quad \eta_0 = 4.618$$

Laminar flows can be derived by setting $\mu_t = 0$ and omitting the equations for $k$ and $\varepsilon$. The associated boundary conditions for velocity and temperature are (see Fig. 1):

at the inflow

$$T = T_a \tag{9}$$

on the insulated wall

$$u = v = 0, \quad \partial T/\partial x = 0 \tag{10}$$

on the heated wall

$$u = v = 0, \quad q'' = q''_{in} \tag{11}$$

At the first inner grid point, the following standard equations are used to predict the turbulent kinetic energy, $k_{in} = a \cdot U^2_{in}$, and its dissipation, $\varepsilon_{in} = \rho C_\mu (k^2/R\mu)$. The following standard constants are used in the above equations, $a = 0.01$ and $R = 10$.

The governing equations, eqns 1–8, for the present study are solved by the finite element code FIDAP with a pressure-projection method introduced in Fluid Dynamics International.[4] The segregated iterative solver is used to solve the transport

variables $u, v, T, k, \varepsilon$, and $p$. To overcome the difficulty of numerical convergence and instability, solutions are obtained by employing hybrid upwinding and relaxation schemes. The hybrid relaxation factors are maximum 0.1 and minimum 0.01 for $u, v, k$, and $\varepsilon$, and maximum 0.05 and minimum 0.01 for, $T$. The local criterion for numerical convergence, i.e. the maximum relative difference between two consecutive iterations for any local variable, is less than $10^{-3}$. Convergence is typically achieved after about 250 iterations with a central processing time of four h on the Dec 3000–900 AXP computer.

Non-uniform grids are used both in $x$ and $y$-directions. A large number of grid points are placed at geometrically decreasing distances in the region next to the walls, where specially large gradients of velocity and thermal gradients are expected. Four-node quadrilateral elements are used. A different number of grid points are tested and the resulting flow rate and heat balance from these tests are compared, to check the accuracy of the solution. A grid system of $79 \times 231$ nodes is found sufficient for the solutions presented here.

## 4. Numerical and experimental results

The numerical results presented here are obtained for constant uniform input heat flux, $q''_{in}$, varying from 20 to 500 W/m$^2$. Effects of the emissivity of the bounding surfaces are also analysed on the thermal behaviour of the air passing through the gap. The ambient air temperature is 293 K and the Prandtl number is $Pr = 0.708$. Other important parameters are the height of the heated wall and the insulated wall which are 6.5 and 7.0 m, respectively. The thermal properties of the air are calculated at the reference temperature of 300 K.

### 4.1. *Flow and heat transfer at different constant uniform input heat flux*

The outlet air velocity and outlet air temperature profiles as well as the surface temperatures of the heated and insulated walls of the air gap subjected to a uniform input heat flux 20, 300, and 500 W/m$^2$ are presented in Figs 2 and 3. The corresponding, $Ra_d = g\beta q''_{in} d^4/\nu\alpha_H\lambda$, for the present cases are, $2 \times 10^8$, $3 \times 10^9$ and $5 \times 10^9$, respectively. These $Ra_d$ numbers are based on the separation distance of the gap, $d = 0.23$ m.

Figure 2(a) and (b) show the outlet air velocity and temperature profiles. At 20 W/m$^2$, the flow is assumed to be laminar. It can be noted that the convective flow induced by the horizontal temperature gradient is very weak, and it will be shown later that the radiation heat transfer between surfaces is a dominating mechanism. Two boundary layers are developed along the heated and insulated walls. At a large part of the outlet cross section area the outlet air temperature is equal to the ambient temperature. By increasing the $Ra_d$ number, the flow characteristic of the air will be changed. For 300 and 500 W/m$^2$ the flow is assumed to be turbulent. This case is dominated mainly by the turbulent convection heat transfer. This effect is due to the fact that the heat is mostly convected from the heated wall to the insulated wall by a

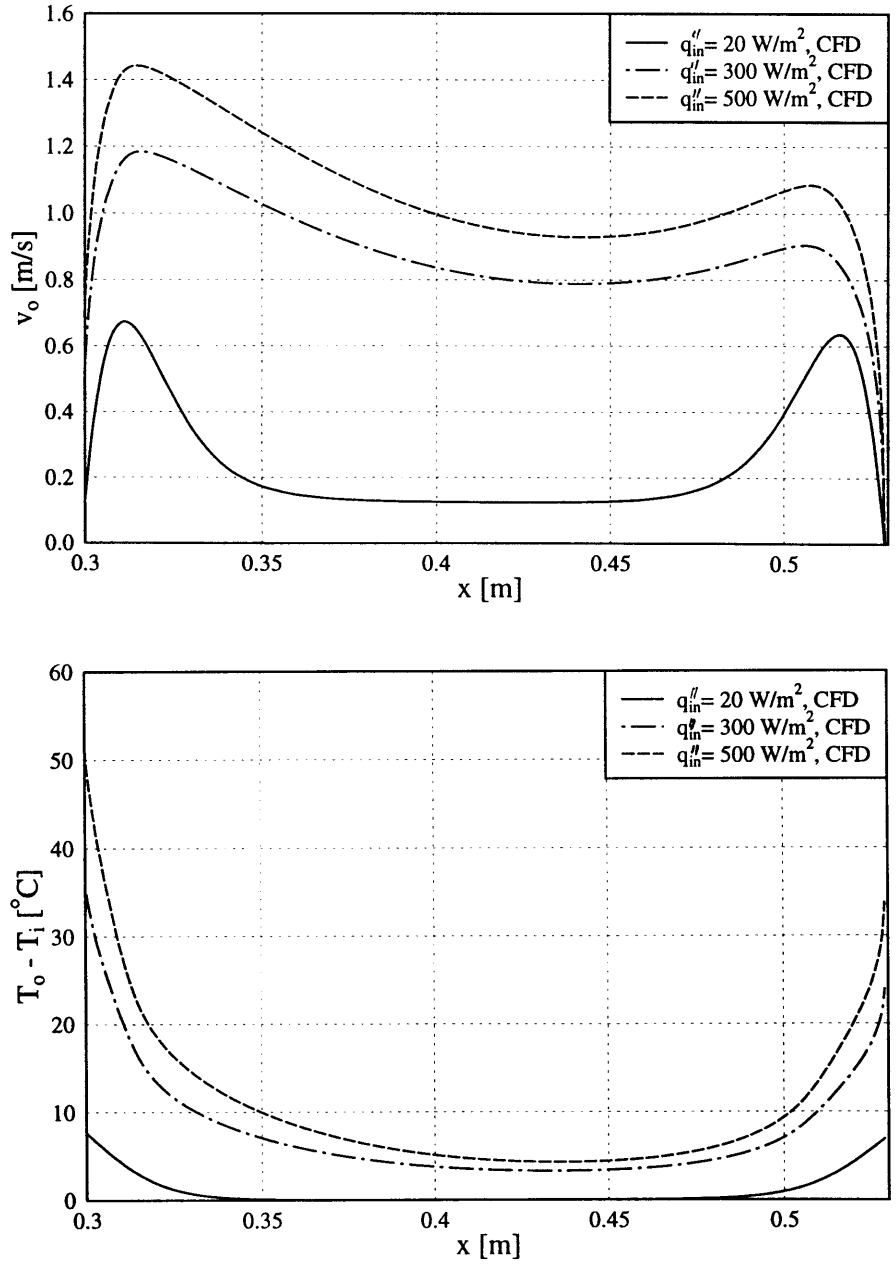


Fig. 2. (a) $y$-component velocity profile of the air at the outlet of the gap, $v_o$, and (b) the outlet air temperature profiles, $T_o - T_i$.

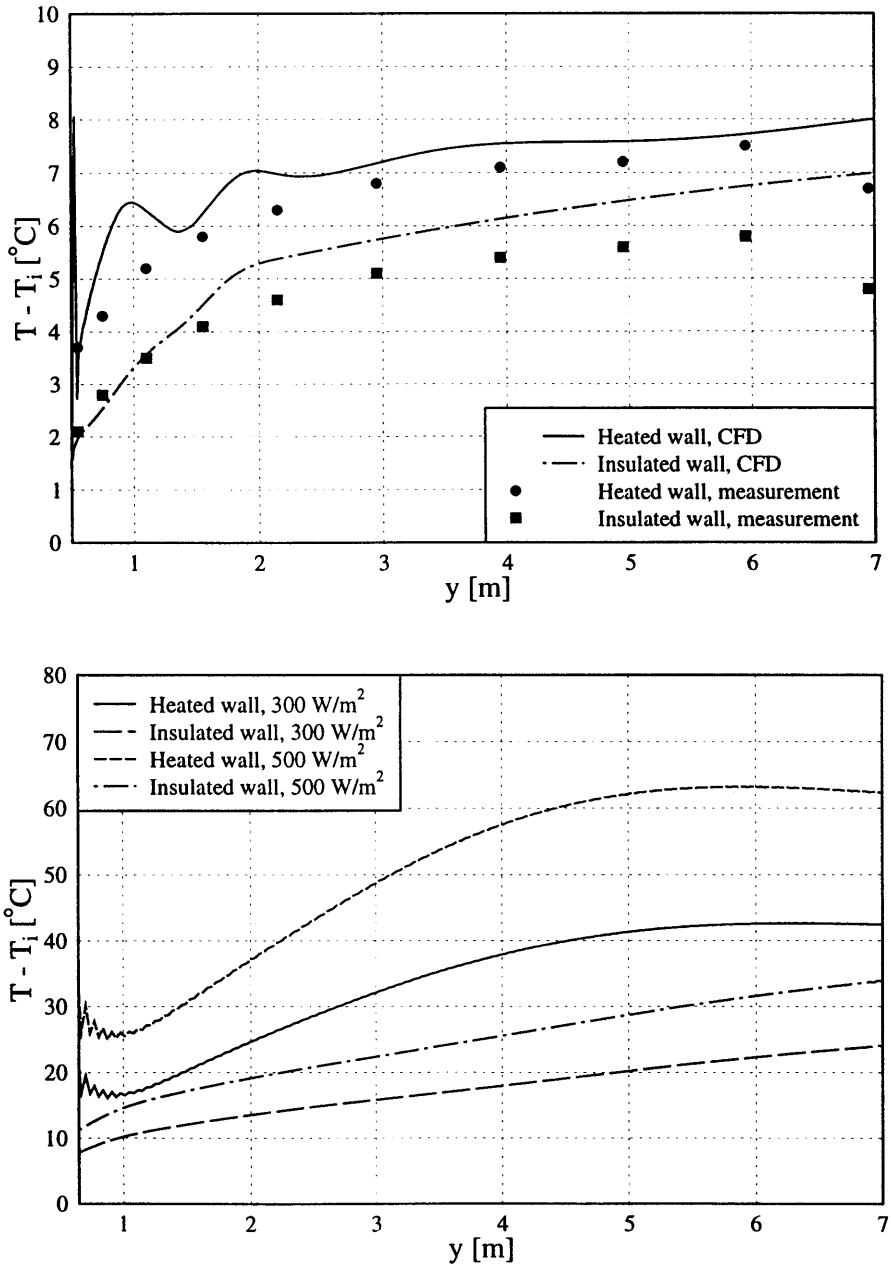


Fig. 3. Surface temperature of the heated and insulated walls, (a) $q''_{in} = 20$ W/m$^2$ and (b) $q''_{in} = 300$ and 500 W/m$^2$.

very strong turbulent convection along the horizontal cross section area. According to Fig. 2(a), there is two-peak velocity close to the heated and insulated walls, but the velocity profile of turbulent case has a tendency to be more flattened.

Figure 3(a) shows the surface temperature of the heated and insulated walls for $q''_{in} = 20\ W/m^2$. The experimental results are also presented in Fig. 3(a). The instability tendencies in temperature values at the lower part of the heated wall can be a reason of the separation effect close to the lower edge of the heated wall. For the turbulent cases ($q''_{in} = 300$ and $500\ W/m^2$) Fig. 3(b), the surface temperatures increase very fast along the height of the channel, compared to the laminar case where the changes are very slow. It is also interesting to note that the temperature difference, between the heated and insulated wall along the height of the channel is almost constant for the laminar case, while for the turbulent flow the temperature differences increase along the height of the channel. The numerical predictions agree well with the results from the measurements for the laminar case, as shown in Fig. 3(a).

Figure 4(a) and (b) show the variation of the average outlet air velocity and the outlet air temperature as a function of the input heat flux. The outlet air velocity and temperature are found to have a linear relation with the input heat flux for the turbulent cases in the log-log scale. A linear regression analysis is performed in the log-log scale and the fitted results are presented in the legends of Fig. 4(a) and (b). It can be seen that the power law expression provides an excellent representation of the numerical results. For comparison the experimental results and the lumped parameter analysis are also included in Fig. 4(a) and (b).

Based on the lumped parameter analysis for fully turbulent flow, the power law relation between velocity and input heat, and between the temperature rise at the outlet of the gap and the input heat raised to an exponent equal to 1/3 and 2/3 respectively, see eqns (12) and (13), compared to 0.353 and 0.654 for the numerical predictions. A more detailed analysis of the lumped parameter method will soon be presented by authors. For the experimental data for, $q''_{in}$, varying from 200 to 300 $W/m^2$ the exponent is 0.34 for the relation between outlet velocity and input heat. This is within the measurement accuracy equal to the theoretical value.

$$U_o = \left(\frac{\alpha H}{A_i \psi}\right)^{1/3} B^{1/3} \tag{12}$$

$$\Delta T_b = T_o - T_i = \frac{1}{g\beta}\left(\frac{\psi}{\alpha H A_i^2}\right)^{1/3} B^{2/3} \tag{13}$$

For convenience the following terms have been introduced, specific buoyancy flux, $B = g\beta q/\rho C_p$, and, $\psi = \rho(1/\rho_0 - 1/\rho_i) + \lambda H/d + 0.5(1 + k_{entr})$. The result from the lumped parameter analysis is based on the friction coefficient, $\lambda = 0.024$, and the entrance loss, $k_{entr} = 0.5$, which is the standard value for a sharp-edged inlet. These input parameters predict a velocity somewhat higher than the recorded velocities. One plausible explanation is that the entrance losses are larger because the inlet is a 90° bend, see Fig. 1.

The numerically determined average heat transfer coefficient on the heated and

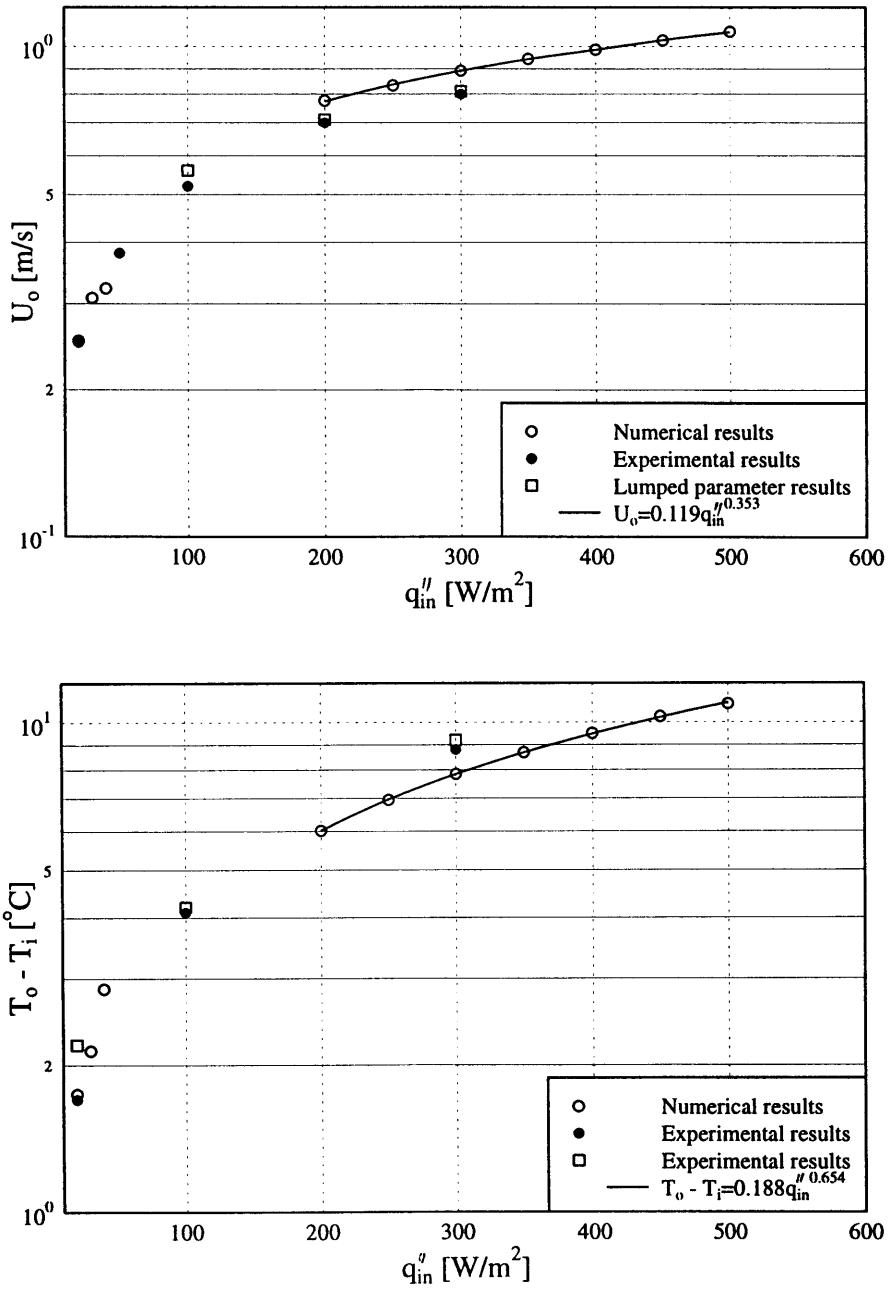


Fig. 4. Comparison of experimentally and numerically determined outlet air velocity (Fig. 4(a)) and temperature (Fig. 4(b)) results. The square shown in Fig. 4(b) is the recorded temperature difference while the filled circle shows the obtained temperature difference based on input heat and recorded flow rate.

insulated walls at a different input heat flux are plotted in Fig. 5 as a function of, $q''_{in}$. For fully turbulent flow cases, i.e. for, $q''_{in}$, varying from 200 to 500 W/m$^2$ (corresponding to a $Ra_H$ number varying between $1.3 \times 10^{15}$ to $3.2 \times 10^{15}$ based on the height of the heated wall), the best fitted lines showed that the power exponent between, $h_h$ and $q''_{in}$, and, $h_c$ and $q''_{in}$, is equal to 0.247 and 0.228, respectively. The exponents are in good agreement with the result presented in Vliet and Liu.[5] The results are presented in the legends of Fig. 5.

The percentage of the input heat which is dissipated to the air via convection and via radiation to the bounding surfaces is show in Fig. 6. The results show that the magnitude of the radiative heat transfer is comparable to the convective term at low, $q''_{in}$, but it has a tendency to decrease by increasing the input heat flux. For input heat flux 200 W/m$^2$ more than 67% of the input heat is transferred to the air via convection and it is increasing very slowly by increased input heat flux.

### 4.2. *Flow and heat transfer at different emissivity of the bounding surfaces*

The relative flow rate through the gap decreases by reducing the emissivity of the bounding surfaces, but on the other hand, the average outlet air temperature increases (the input heat flux is constant), see Table 1. In other words, the cooling capacity of the cavity will be reduced and result in a lower efficiency for the panel. It can be seen also from Table 1 that the emissivity of the bounding surfaces strongly influences the surface temperature of the insulated and heated walls. The difference between the

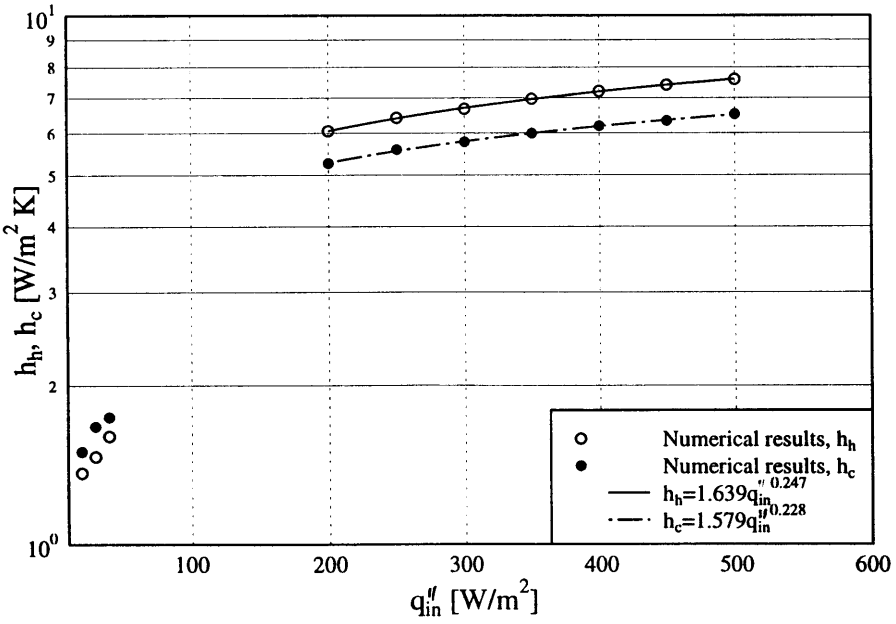


Fig. 5. Average heat transfer coefficient for the heated and insulated wall.

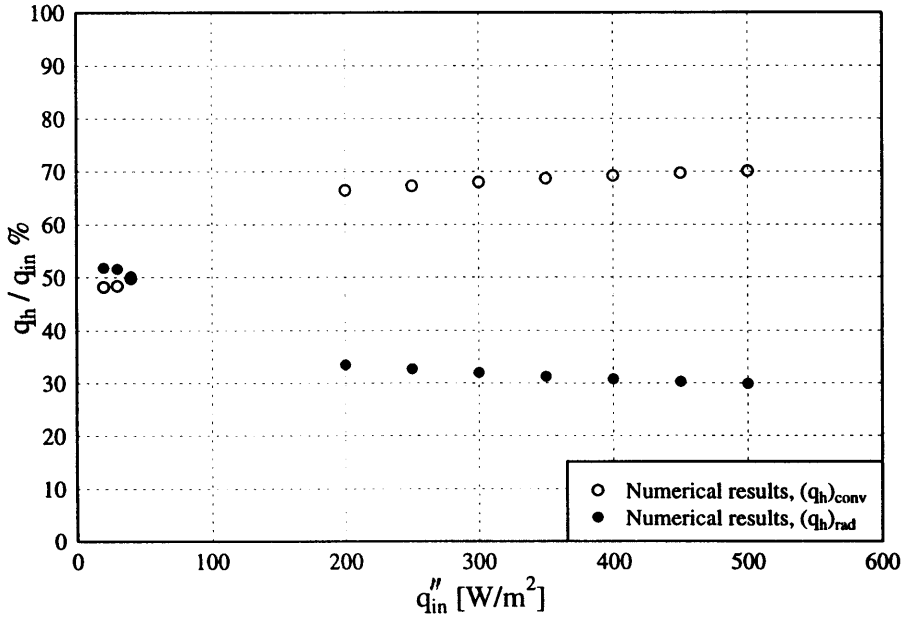


Fig. 6. The amount of the heat transferred from the heated wall to the air by means of convection and radiation.

average surface temperature of the heated wall for case one and four is more than 14°C. This temperature rise will reduce the efficiency of the solar cell by 0.6%. The fact is that the amount of radiative heat transferred from the heated to the insulated wall will be reduced by increasing the thermal resistance due to the radiation. For surfaces with a lower emissivity factor most of the input heat will be transferred directly from the heated wall via convection to the air. For the pure convection case ($\varepsilon_h = \varepsilon_c = 0$) the radiative heat flux is zero and the consequence is that the convection term for the insulated wall can be neglected, the surface temperature of the insulated wall is close to the air temperature adjacent to the wall and the surface temperature of the heated wall will rise to the highest possible temperature.

The results also indicate that the amount of radiation heat penetration through gap openings is also reduced from case one to four. In other words, using surfaces with lower emissivity factor will allow the convective heat transfer to dominate the heat transfer mechanism while the radiation heat exchange between surface boundaries will be diminished. The effect of the separation distance, *d*, on the thermal behaviour of the air was presented in an earlier report by the authors, see Moshfegh and Sandberg[6] and Sandberg and Moshfegh[7].

## 5. Conclusions

An investigation was made to provide better understanding of the mechanism of heat transfer in the air gap behind PV panels by means of both numerical and

Table 1
Effect of emissivity of the bounding surfaces on the channel flow and thermal characteristics

| Case | $\varepsilon_h$ | $\varepsilon_c$ | $\bar{T}_o$ °C | $\bar{U}_o$ m/s | $\bar{T}_h$ °C | $\bar{T}_c$ °C | $\bar{h}_h$ W/m$^2$K | $\bar{h}_c$ W/m$^2$K | $(q_h)_{conv}/q_{in}$ % | $(q_h)_{rad}/q_{in}$ % | $(q_o-q_i)_{conv}/q_{in}$ % | $(q_o+q_i)_{rad}/q_{in}$ % |
|---|---|---|---|---|---|---|---|---|---|---|---|---|
| 1 | 1.0 | 1.0 | 27.8 | 0.89 | 50.6 | 35.0 | 6.7 | 5.8 | 68.0 | 32.0 | 97.8 | 2.2 |
| 2 | 1.0 | 0.1 | 28.3 | 0.83 | 62.7 | 24.3 | 6.3 | 5.0 | 89.4 | 10.6 | 96.6 | 3.4 |
| 3 | 0.1 | 1.0 | 28.5 | 0.84 | 64.2 | 23.9 | 6.3 | 5.6 | 93.4 | 6.6 | 99.8 | 0.2 |
| 4 | 0.1 | 0.1 | 28.7 | 0.82 | 65.2 | 22.0 | 6.4 | 4.9 | 96.2 | 3.8 | 99.8 | 0.2 |

$d = 0.23$ m, $H = 6.5$ m, $Pr = 0.708$, $Ra_d = 3.10^9$, $T_i = T_a = 20$°C, $q''_{in} = 300$ W/m$^2$

experimental method. For vertical channels, $U_o$ and $T_o$ increases by increasing the input heat flux. However, for a fixed input heat flux, $U_o$ decreases by using surfaces with lower emissivity factor, due to the increments in temperatures at the outlet of the channel, $T_o$. In terms of efficiency of the solar panel, an indication that is beneficial to have surfaces with high emissivity factor.

For fully turbulent flow, $U_o$ and $T_o$, are according to the numerical predictions proportional to the, $q''^{m}_{in}$, where $m$ is 0.353 and 0.654, respectively. For the $200 \leqslant q''_{in} \leqslant 500$ W/m$^2$, $h_h$ and $h_c \propto q''^{n}_{in}$, where $n$ is 0.247 and 0.228, respectively. According to the measurements for the interval $200 \leqslant q''_{in} \leqslant 300$ W/m$^2$ the exponent, $m$, is 0.34 for $U_o$. The exponents show good agreement between the numerical predicted results and the experimental results.

The analysis revealed the importance of radiation heat exchanges for the heat transfer mechanisms between the channel walls. For input heat flux equal or more than 200 W/m$^2$ nearly 30% of the input heat is transferred to the otherwise unheated wall via radiation and then it is dissipated to the air through convection.

## Acknowledgements

The experimental data used in this paper were obtained in a project carried out for European Joint Research Centre, Italy. The authors gratefully acknowledge the funding received from European Joint Research Centre, Italy, through Contract No. EU 10544-94-11 F1PC ISP S. The authors also acknowledge the help at various stages of the project from the following members of the staff at The Royal Institute of Technology, KTH, Gävle, Sweden, C. Blomqvist, H. Lundström, M. Mattsson, L. Smids, R. Peltari and T. Persson.

## References

[1] Etheridge D, Sandberg M. Building ventilation theory and measurements. John Wiley & Sons, Chichester, UK, 1996.

[2] Gray DD, Giorgini A. The validity of the Boussinesq approximation for liquids and gases. Int J of Heat and Mass Transfer 1976;19:545–551

[3] Yakot V, Orszag SA, Thangam S, Gatski TB, Speziale CG. Development of turbulence models for shear flows by a double expansion technique. Physics of Fluids 1992;A4(7):1510–1520.

[4] Fluid Dynamic International, Evanston, IL. FIDAP version 7.51 1995.

[5] Vliet GC, Liu CK. An experimental study of turbulent natural convection boundary layers. J of Heat Transfer November 1969;517–531.

[6] Moshfegh B, Sandberg M. The investigation of fluid flow and heat transfer in a vertical channel heated from one side by PV elements. Part I—Numerical Study. Proceedings of The Fourth Renewable Energy Congress, Denver, USA 1996.

[7] Sandberg M, Moshfegh B. The investigation of fluid flow and heat transfer in a vertical channel heated from one side by PV elements. Part II—Experimental Study. Proceedings of The Fourth Renewable Energy Congress, Denver, USA 1996.